High-Acoustic-Impedance Tantalum Oxide Layers for Insulating Acoustic Reflectors

Jose Capilla, Jimena Olivares, Marta Clement, Jesús Sangrador, Enrique Iborra, and Arnaud Devos

Abstract—This work describes the assessment of the acoustic properties of sputtered tantalum oxide films intended for use as high-impedance films of acoustic reflectors for solidly mounted resonators operating in the gigahertz frequency range. The films are grown by sputtering a metallic tantalum target under different oxygen and argon gas mixtures, total pressures, pulsed dc powers, and substrate biases. The structural properties of the films are assessed through infrared absorption spectroscopy and X-ray diffraction measurements. Their acoustic impedance is assessed by deriving the mass density from X-ray reflectometry measurements and the acoustic velocity from picosecond acoustic spectroscopy and the analysis of the frequency response of the test resonators.

I. INTRODUCTION

BULK acoustic wave resonator technology is a recent solution for low-cost, high-performance bandpass filters for digital wireless communications, such as wireless networking, cellular phones, or global positioning systems. These filters are composed of several resonators electrically connected to achieve the desired filter characteristics. To obtain well-performing devices, a good acoustic isolation of the resonators is required to avoid energy losses through the substrate that reduce their quality factor (Q). There are two typical methods to achieve a good acoustic isolation. The first method consists of creating an air gap between the resonator and the substrate; because the acoustic radiation to the air is minimal, energy losses can only take place through the supports. These structures, called film bulk acoustic resonators (FBAR), have some drawbacks; they require complex fabrication technology and exhibit a too-high thermal isolation that limits power handling. The alternative method is the use of acoustic reflectors between the resonators and the substrate; the resulting structures are called solidly mounted resonators (SMR) [1]. Bragg mirrors are typical acoustic reflectors formed by alternating quarter-wavelength-thick layers ($\lambda/4$-layers) with low and high acoustic impedance [2].

J. Capilla, J. Olivares, M. Clement, J. Sangrador and E. Iborra are with the Grupo de Microsistemas y Materiales Electrónicos del Centro de Materiales y Dispositivos Avanzados para las Tecnologías de la Información y Comunicaciones (GMME-CEMDATIC), Universidad Politécnica de Madrid, Madrid, Spain (e-mail: mclement@etsit.upm.es).

A. Devos is with the Institut d'Électronique, Microélectronique et Nanotechnologie, Institut Supérieur d'Électronique et du Numérique, UMR Centre National de la Recherche Scientifique 8520, Lille, France.

The acoustic isolation achieved (reflection coefficient) increases with the number of layers and with the mismatch between the acoustic impedances of two consecutive layers. Considering that the acoustic impedance of a given material is the product of the longitudinal sound velocity and the mass density, these two material properties must be perfectly known to set the thickness of the films to $\lambda/4$ to get the targeted resonant frequency and to fix the number of layers required for a specified mirror reflectance. Table I summarizes the experimental values of such material properties for the most commonly used acoustic mirror constituents.

Silicon dioxide (SiO_2) is commonly used as a low-acoustic-impedance material, because it is easy to process and fully compatible with standard silicon technologies [3]. Other low-impedance materials are Al [4] and SiOC [5], although they are less frequently used because of the metallic character of Al and the elevated acoustic losses of SiOC. On the other hand, materials with high acoustic impedance are typically high-density metals exhibiting, additionally, a sufficient sound velocity, such as Ir [6], Mo [7], or W [8]. If these high-impedance layers are replaced by insulating films, the fabrication process of BAW filters can be significantly simplified, because there is no need to define the continuous metallic layers that short circuit the different resonators built on top of the same acoustic mirrors. Achieving insulating Bragg mirrors thus requires high-acoustic-impedance insulating layers, which are, unfortunately, not easily available. So far, insulating acoustic mirrors have been obtained by combining SiO_2 or SiOC layers with AlN [9], Si_3N_4 [5], or Ta_2O_5 [10], [11], although the acoustic properties of this last material have not been extensively characterized. However, none of these three materials exhibits really high acoustic impedances, compared with that offered by high-density metallic layers. The considerably high acoustic velocity of AlN combined with a low mass density (see table I) provides a moderate acoustic impedance. On the other hand, Ta_2O_5 films offer acoustic impedance similar to AlN by virtue of its high mass density, although the sound velocity appears to be considerably lower.

In this work, we have characterized the acoustic properties of TaO_x (with x close to 2.5) films to investigate whether these layers, in combination with SiO_2 films, may provide better acoustic isolation than SiO_2/AlN-based Bragg mirrors. The structure, mass density, and sound velocity of sputtered TaO_x films have been assessed by different techniques, which include the fabrication and characterization of specific devices for the evaluation of its sound velocity.

TABLE I. ACOUSTIC IMPEDANCE OF METALLIC AND INSULATING MATERIALS.

Material	Mass density $(kg \cdot m^{-3})$	Sound velocity $(m \cdot s^{-1})$	Acoustic impedance $(kg \cdot m^{-2} \cdot s^{-1})$
SiOC	1500	2400	3.6×10^6
Al	2700	5100	11.2×10^6
SiO_2	2200	6000	13.2×10^6
Si_3N_4	2200	9900	21.8×10^6
AlN	3300	11000	36.3×10^6
Mo	10300	6190	63.8×10^6
W	19290	5180	99.9×10^6
Ir	22500	5300	119.2×10^6

II. EXPERIMENT

A. Sputtering Process

TaO$_x$ films were deposited in a Leybold Z-550 system (Leybold AG, Köln, Germany) by pulsed-dc magnetron sputtering of a 150-mm-diameter Ta target in Ar/O$_2$ admixtures. A pulsed-dc power of 50 kHz and duty cycle 75% was applied to the target. Up to 150 films were deposited under different conditions by varying the total pulsed-dc power between 500 and 1200 W, the total pressure in the chamber between 1.5 and 3.3 mTorr, and the percentage of O$_2$ in the gas between 30% and 100%. An RF source was used to polarize the substrate between -50 V (with no RF power applied to it) and -150 V. The substrates were not intentionally heated before or during deposition.

The sputter process of a Ta metallic target in Ar/O$_2$ atmospheres shows a transitory behavior resulting from the oxidation of the target. When bombarding a clean Ta metallic surface at constant power with a gas containing a certain percentage of oxygen (less than 100%), the time to stabilize the plasma impedance can reach several hours. To guarantee that the target had reached a stationary state before starting deposition, the target was first preconditioned at the deposition power in pure oxygen atmosphere; the voltage of the cathode attained a constant value after around 15 min, when the plasma impedance reached the steady state. The selected gas mixture was then fed into the chamber at the chosen pressure and the voltage of the cathode controlled until the new steady state was attained (15 to 30 min). At this moment, the shutter was opened for film deposition for the desired time. Subsequent depositions under identical conditions required only a few minutes for stabilization. Every time the deposition conditions were modified, the complete conditioning process was restarted. The TaO$_x$ films were deposited on (100) silicon wafers for IR transmission measurements and on acoustic reflectors (described below) built on top of silicon substrates for the assessment of the sound velocity through the frequency response of test SMRs.

B. Film Characterization

The structure and morphology of the 150 TaO$_x$ films were evaluated by infrared transmission measurements carried out with a Nicolet 5-PC Fourier transform infrared (FTIR) spec-

trophotometer (Thermo Scientific, Waltham, MA), which provided a straightforward assessment of the chemical bonding configuration of the films. We used non-polarized light at normal incidence over the 400 to 4000 cm^{-1} range with a spectral resolution of 4 cm^{-1}. The absorption bands corresponding to the Si substrate were eliminated by subtracting the absorbance spectrum measured in bare Si. X-ray diffraction patterns of 20 representative films were measured in conventional Bragg–Brentano geometry in a Supratech XPert MRD diffractometer (Panalytical, Almelo, The Netherlands) between $2\theta = 10°$ and $2\theta = 80°$.

The assessment of the acoustic properties of TaO$_x$ films requires very precise measurements of their mass density, acoustic velocity, and thickness. The thickness of the TaO$_x$ films and that of the other films involved in test devices were measured with a Dektak 150 profilometer (Veeco Instruments, Plainview, NY). The density of the TaO$_x$ layers was assessed by X-ray reflectometry (XRR) measurements using the same diffractometer operated at grazing incidence between $\theta = 0.05°$ and $\theta = 2.5°$. Finally, the longitudinal sound velocity was assessed using two different techniques. First, the sound velocity was measured in different test structures by the picosecond ultrasonic technique [12]. A second assessment was deduced from the frequency response of the electrical impedance of specific SMR test devices built on top of acoustic reflectors containing the TaO$_x$ layers under study; this was measured with an Agilent PNA N5230A network analyzer (Agilent Technologies Inc., Santa Clara, CA). TaO$_x$ films with thickness ranging between 150 and 1000 nm were inserted between a well-characterized acoustic reflector, composed of four alternating porous-SiO$_2$ [13] and Mo films, and a Mo/AlN/Mo resonator, as shown in Fig. 1. The excitation of the resonator induced a $\lambda/2$ resonance in the TaO$_x$ film. The fitting of the experimental data with Mason's model allowed derivation of the longitudinal acoustic velocity, provided that the material properties and the thickness of all the layers involved in the device were well known.

III. RESULTS AND DISCUSSION

A. Structure and Composition of Sputtered Tantalum Oxides

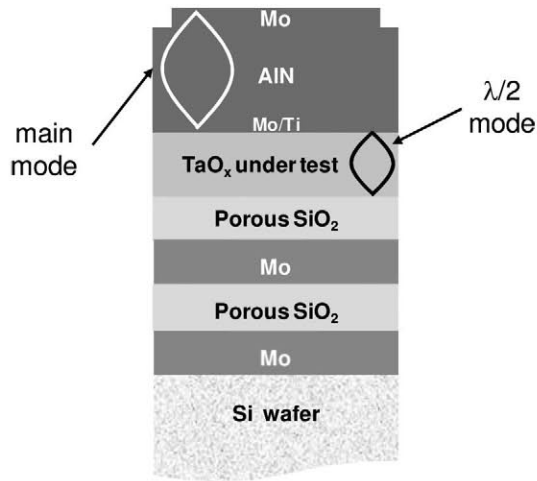Fig. 2 shows the IR transmission spectra of three TaO$_x$ films of different thickness. The bands at 950 and 650 cm^{-1}

Fig. 1. Sketch of the test devices used for assessing the sound velocity in sputtered TaO_x films. The main resonant mode in the piezoelectric stack is represented in white, and the $\lambda/2$ mode in the TaO_x film in black.
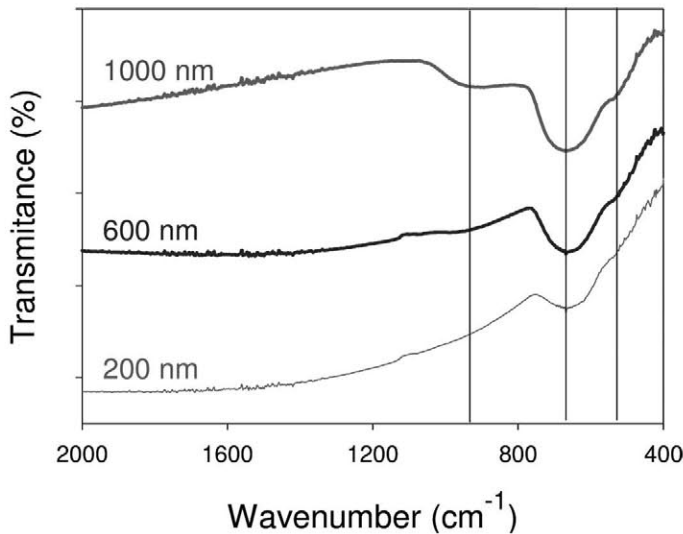

Fig. 2. Infrared transmission spectra between 2000 and 400 cm^{-1} of three TaO_x films of different thickness.

Fig. 3. X-ray diffraction patterns of TaO_x films of different thickness.

have been associated with the Ta-O-Ta stretching mode and with the O≡Ta bond, respectively, of amorphous TaO_x films [14]. The main absorption band at 650 cm^{-1} has been reported to shift to lower wavenumbers (down to 510 cm^{-1}) in polycrystalline films. In our spectra, this band appears as a shoulder in the 530 cm^{-1} region. The spectra suggest that our TaO_x films are mainly amorphous, but contain a certain amount of microcrystals. Considering the amplitude ratio of the bands at 530 and 650 cm^{-1} as a qualitative estimation of the amount of microcrystals embedded in the amorphous matrix, a slight increase is observed with the thickness of the films. However, in films of similar thickness, we have not observed any clear dependence between the amount of microcrystals and the deposition conditions used in this work.

X-ray diffraction measurements confirm this behavior. Fig. 3 shows the XRD patterns of the three TaO_x films of different thickness analyzed by FTIR. It is important to

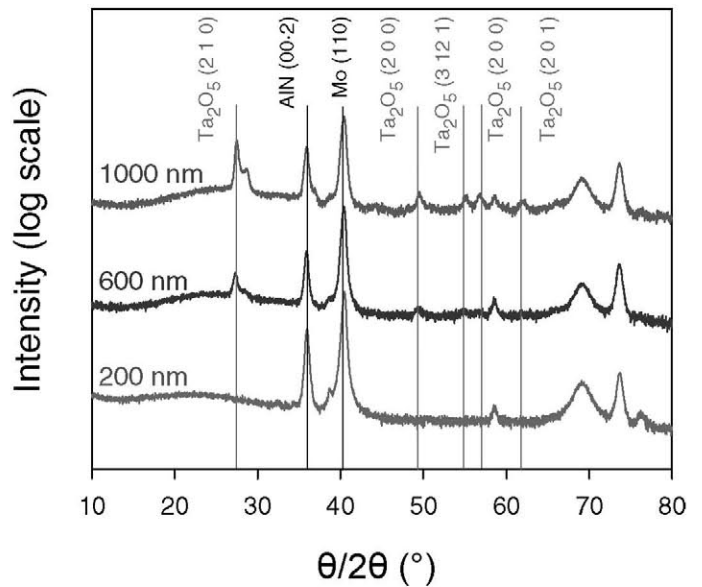note that, among all the films deposited, only a few exhibited clear XRD peaks corresponding to the orthorhombic β-phase of Ta_2O_5, whereas most of the films deposited in similar conditions were clearly amorphous. Peaks at $2\theta = 26°$, $52°$, $48°$, $56°$, and $62°$ corresponding to the (210), (200), (3121), (200), and (201) directions of the Ta_2O_5 orthorhombic β-phase appear in the patterns corresponding to the thicker films, whereas no traces of these peaks are visible in the thinner one, which indicates its amorphous character. Additional peaks corresponding to AlN and Mo are also observed, because the films are characterized after depositing the piezoelectric stack for electric characterization. The data suggest again that thicker films tend to contain some nanocrystals whose grain size, derived from the width of the TaO_x peaks, is around 10 nm. However, we have not found any clear trend between the microcrystalline character of the samples (or any other film property) and the deposition conditions.

B. Density Assessment

The mass density (ρ) of the TaO_x films was measured by XRR, which provides a direct assessment of ρ, independent of the thickness. X-rays impinging on smooth TaO_x surfaces at grazing incidence below a critical angle (θ_c) are totally reflected. When the incident angle exceeds θ_c, the X-rays penetrate into the film and the intensity of the reflected beam drops sharply. According to [15], ρ can be obtained through the measured θ_c. The XRR measurements corresponding to the films exhibiting the greatest and the lowest density are shown in Fig. 4; the curves of all the remaining films lie between these two traces. The experimental data were fitted using the commercial software RCREFSimW (Innovations for High Performance Microelectronics, Frankfurt, Germany) which provided an accurate value of ρ. The values obtained were 8100 and 7300 kg·m^{-3}, respectively, revealing that even the denser
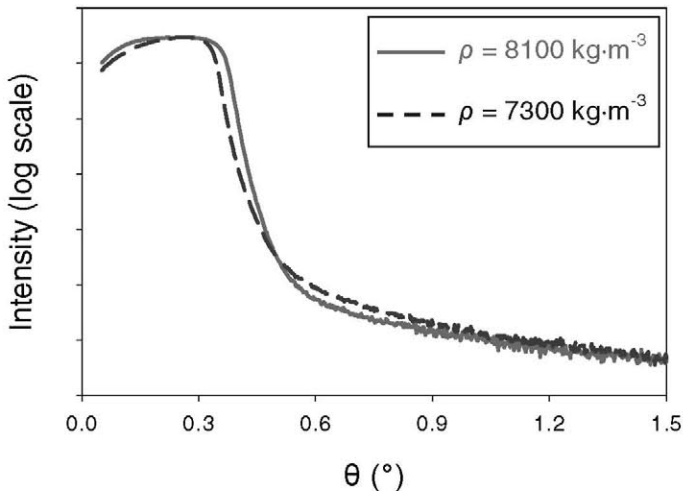
Fig. 4. X-ray reflection curves of two 200-nm-thick TaO_x films grown on acoustic reflectors. The solid line corresponds to the film of highest mass density and the dashed line corresponds to the film of lowest mass density.
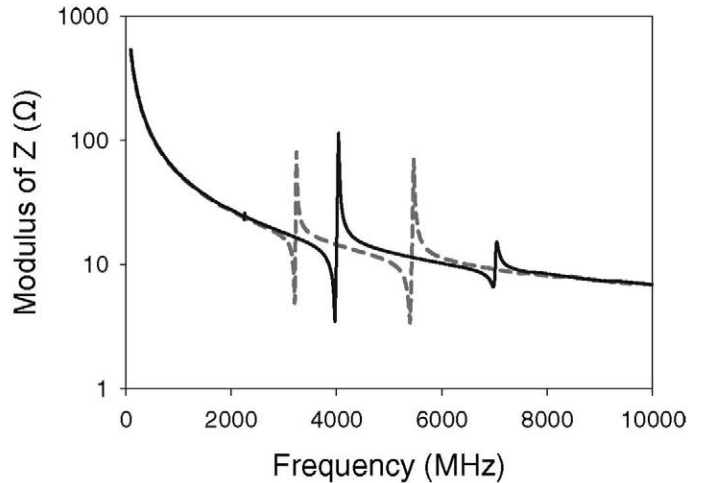

Fig. 5. Modulus of the impedance versus frequency of two otherwise identical test SMRs containing 180-nm-thick (solid line) and 400-nm-thick (dashed line) TaO_x films.

films do not reach the nominal mass density of Ta_2O_5 (8200 kg·m^{-3}). These low values of ρ could be associated either with a lack of stoichiometry (films containing oxygen in excess) or, more likely, with a non-packed structure associated with the amorphous structure of most of the films. The high value of the refractive index (2.26) measured at a wavelength of 400 nm confirms this hypothesis.

C. Sound Velocity Assessment

1) Assessment Through Test SMRs: The first way to assess the longitudinal sound velocity in the TaO_x films consisted of the measurement of the $\lambda/2$ resonant mode induced in these layers when they were placed in intimate contact with a piezoelectric resonator, as shown in Fig. 1. Taking into account that the wavelength of the stationary wave of this mode is ideally twice the thickness of the layer, the sound velocity v_s can be estimated, in a first approach, from the resonant frequency f_0 of the $\lambda_{TaOx}/2$ mode and the thickness t of the layer through

$$v_s = f_0 \times 2 \cdot t. \tag{1}$$

However, because the resonant frequencies of all of the modes also depend on the weight of the different layers involved in the test SMR, reliable values of the longitudinal sound velocity were only achieved if the whole experimental frequency response of the test resonator was fitted with Mason's physical model [16].

The variation with frequency of the modulus of the electrical impedance of two representative test SMRs containing TaO_x layers of different thickness is shown in Fig. 5. Two resonances appear in each spectrum at different frequencies. The low-frequency modes correspond to the main resonance in the AlN layer, whereas the high-frequency modes are associated with the $\lambda/2$ mode in the

TABLE II. MATERIAL CONSTANTS FOR SOLIDLY MOUNTED RESONATOR MATERIALS.

Material	v_s (m/s)	ρ (kg·m^{-3})
Mo	6290	10 300
SiO_2	5350	1900
AlN	11 000	3300

TaO_x film. Fig. 5 shows that upon decreasing the thickness of the TaO_x film, the two main resonances shift to higher frequencies, not only because of the lower value of $\lambda/2$ but also as a consequence of the reduction of the weight of this layer, which also affects the propagation of the wave in the whole structure.

Fitting the experimental data to Mason's model requires precise values of the material properties of all layers involved in the test structures and of all the dimensions of the devices (thickness of layers and areas of the resonators). The areas of the top electrodes, which defined the areas of the SMRs, were measured carefully with an optical microscope to avoid errors resulting from the undercutting during the electrode definition. The properties of the different materials used for fitting the experimental data are listed in Table II. Data for Mo and AlN were taken from the literature and those corresponding to porous SiO_2 had been carefully characterized in a previous work [13]. All these properties have also been routinely tested in other devices that do not contain TaO_x films.

The fitting of the experimental data of Fig. 5 allowed deduction of the values of the longitudinal sound velocity of the different TaO_x layers. These are depicted as a function of the thickness of the TaO_x slab in Fig. 6 along with the value of the sound velocity deduced from the alternative technique described in Section III-C-2.

2) Assessment Through Picosecond Measurements: The aim of these experiments is to measure the time-of-flight (τ) of a longitudinal acoustic wave within the TaO_x films
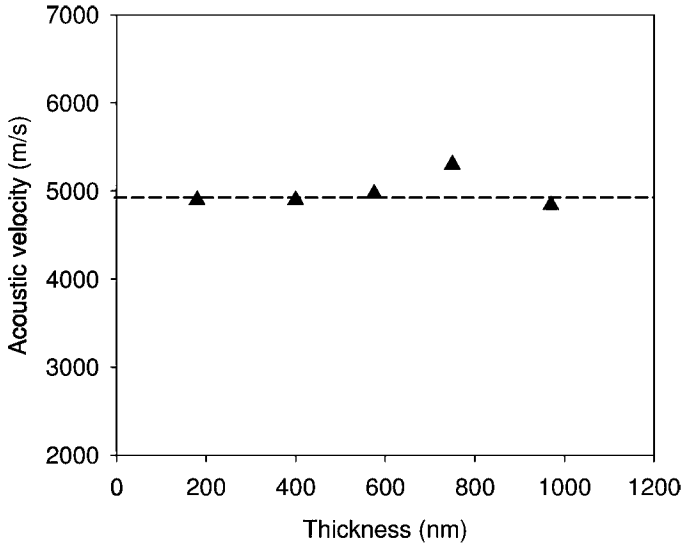
Fig. 6. Sound velocity of a set of TaO$_x$ of different thicknesses grown under identical conditions obtained from BAW devices measurements (triangles). The line shows the mean value obtained by picosecond measurements.
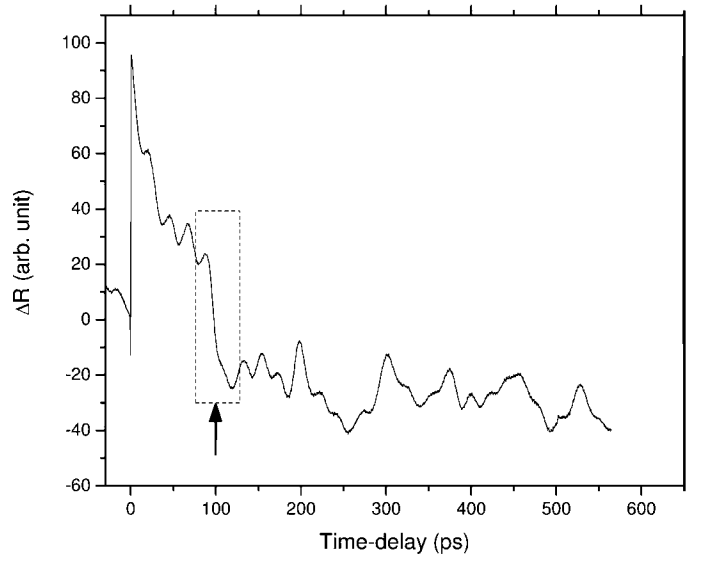
Fig. 7. Reflectivity signal as a function of time obtained in a 180-nm-thick TaO$_x$ layer grown on top of an acoustic reflector. The arrow close to 100 ps shows the sudden step resulting from the reflection of the acoustic pulse at the free surface, corresponding to a single way through the bi-layer SiO$_2$ and TaO$_x$.

deposited on top of the Bragg mirrors. If the thickness d of the layer is known, the sound velocity is obtained by dividing d by τ. In this experiment, the acoustic wave is generated by means of a pump laser pulse that impinges the surface of the sample; a strong absorption takes place when the laser pulse reaches the first metallic layer it encounters, which produces a local heating of the metallic layer and hence a strain pulse that propagates toward the surface at the longitudinal velocity. The arrival of the acoustic pulse to the surface is detected by using a second laser beam, which allows measurement of the time-of-flight of the acoustic pulse in the layer under study [17]. In our samples, the laser pulse travels through two transparent media (TaO$_x$ and SiO$_2$ films) until it reaches the surface of the first absorbing Mo layer of the acoustic reflector, where the longitudinal strain wave is generated. The acoustic pulse emitted from the buried Mo layer propagates toward the free surface through the transparent SiO$_2$ and TaO$_x$ bi-layer. The arrival of the pulse at the surface is detected as a reflectivity step which is due to the acoustic reflection at the free surface, as shown in Fig. 7. Such a reflectivity step is easily detected, with accuracy better than 2 ps in any structure made of transparent/absorbing layers. A more detailed explanation can be found in [18].

The time delay τ_{exp} deduced in our measurements includes the time-of-flight of the echo through both the SiO$_2$ layer (τ_{SiO2}) and the TaO$_x$ layer ($\tau_{\mathrm{TaO}x}$), and hence can be written as:

$$\tau_{\mathrm{exp}} = \tau_{\mathrm{Ta_2O_5}} + \tau_{\mathrm{SiO_2}} = \frac{d_{\mathrm{Ta_2O_5}}}{v_{\mathrm{Ta_2O_5}}} + \tau_{\mathrm{SiO_2}}.$$

To deduce the sound velocity in the TaO$_x$ slab ($v_{\mathrm{TaO}x}$), we have studied the time delay at which the reflectivity step is observed for a set of TaO$_x$ layers of different thicknesses

($d_{\mathrm{TaO}x}$) deposited on identical acoustic reflectors. Because the SiO$_2$ layer is identical for each sample, by plotting the evolution of the time-delay as a function of the TaO$_x$ thickness and fitting the data using a linear regression (see Fig. 8) we obtain the value of $v_{\mathrm{TaO}x}$ (inverse of the slope) and that of τ_{SiO2} (ordinate at the origin).

The mean value of the sound velocity obtained by this technique is 4900 m·s^{-1}, which is in very good agreement with those achieved by the BAW resonator fitting method (see Fig. 6). The two methods suggest that the 750 nm-thick sample possesses a sound velocity (5300 m·s^{-1}) significantly greater than the other samples, which indicates that there might be some influence of the growth conditions and the structure of the substrates on the properties of the TaO$_x$ films, as suggested by XRD measurements. Indeed, other measurements of $v_{\mathrm{TaO}x}$ carried out in films grown on Si and Mo substrates reveal that $v_{\mathrm{TaO}x}$ tends to be slightly lower in films grown on Si, whereas $v_{\mathrm{TaO}x}$ of films deposited on Mo layers reach greater values (around 5500 m·s^{-1}).

D. Acoustic Reflector Simulations

To investigate whether these TaO$_x$ films may contribute to optimize the performance of insulating acoustic reflectors, we have simulated the acoustic transmittance of mirrors composed of nine alternating layers of porous SiO$_2$ and TaO$_x$ films and compared it with that of conventional AlN-based mirrors. The simulations, shown in Fig. 9, suggest that even for the lowest values of the mass density and acoustic velocity, TaO$_x$-based mirrors exhibit lower transmission coefficients in a wider frequency band than AlN-based reflectors. Additionally, the dispersion of the values of the mass density and acoustic velocity does not
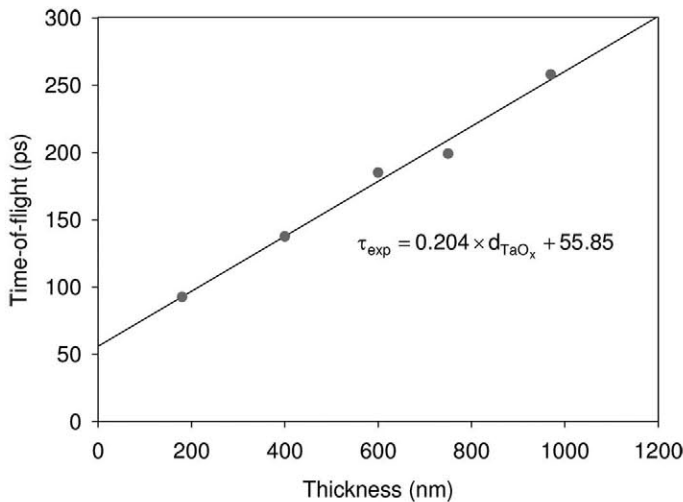
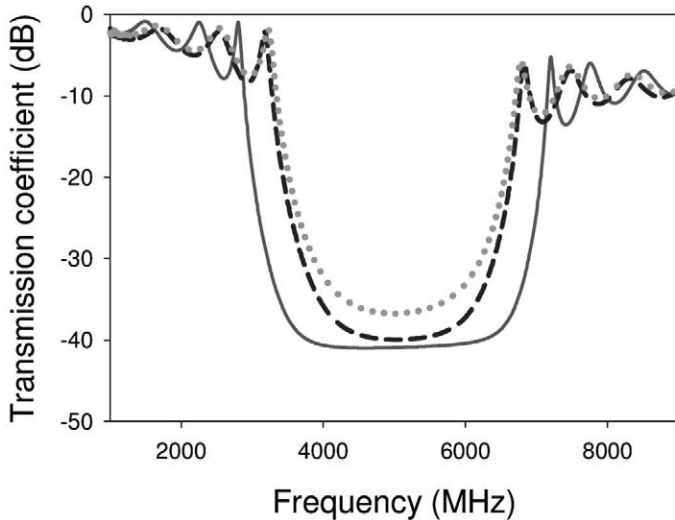Fig. 8. Time of flight for several samples with different TaO_x thickness.

$$\tau_{exp} = 0.204 \times d_{TaO_x} + 55.85$$

Fig. 9. Simulated transmission coefficient of acoustic reflectors composed of nine porous SiO_2/TaO_x layers using the greatest values of ρ and v_s (solid line) and the smallest values of ρ and v_S (dashed line) compared with that of conventional SiO_2/AlN reflectors (dotted line).

affect significantly the performance of the reflectors in the middle of the band.

Preliminary results on the performance of AlN-based SMRs using insulating TaO_x/SiO_2 acoustic reflectors yield quality factors up to 800 at 8 GHz.

IV. CONCLUSIONS

In this paper we have assessed the acoustic properties of TaO_x films deposited at room temperature by reactive pulsed-dc sputtering. The sound velocity derived from picosecond measurements and the frequency response of BAW test devices depends slightly on the thickness of the films, which has been associated with their different structures. Thinner films appear to be amorphous, whereas films that are at least 600 nm thick tend to exhibit some

nanocrystallites. The typical sound velocity in films with thickness below 400 nm is around 4900 m·s^{-1}. The mass density of the TaO_x films was assessed by X-ray reflectometry; the average value is 7600 kg/m^3, around 93% of the nominal density of Ta_2O_5 films. The typical acoustic impedance of the films is 37.2×10^6 kg·m^{-2}·s^{-1}, which is slightly greater than that of AlN. Combined with a low acoustic impedance material, such as porous SiO_2, TaO_x films allow fabrication of all-dielectric acoustic reflectors with good performances for gigahertz-range filtering applications.

REFERENCES

[1] R. Ruby, "Review and comparison of bulk acoustic wave FBAR, SMR technology," in *Proc. 2007 IEEE Int. Ultrasonics Symp.*, pp. 1029–10407.

[2] K. M. Lakin, K. T. McCarron, and R. E. Rose, "Solidly mounted resonators and filters," in *Proc. 1995 IEEE Int. Ultrasonics Symp.*, pp. 905–908.

[3] S. Marksteiner, J. Kaitila, G. G. Fattinger, and R. Aigner, "Optimization of acoustic mirrors for solidly mounted BAW resonators," in *Proc. 2005 IEEE Int. Ultrasonics Symp.*, vol. 1, pp 329–332.

[4] J. Enlund, D. Martin, V. Yantchev, and I. Katardjiev, "Solidly mounted thin film electro-acoustic resonator utilizing a conductive Bragg reflector," *Sens. Actuators A*, vol. 141, pp. 598–602, Feb. 2008.

[5] M. Clement, E. Iborra, J. Olivares, N. Rimmer, S. Giraud, S. Bila, and A. Reinhardt, "DCS Tx filters using AlN resonators with iridium electrodes," *Trans. Ultrason. Ferroelectr. Freq. Control*, vol. 57, no. 3, pp. 518–523, 2010.

[6] J. Olivares, E. Wegmann, M. Clement, J. Capilla, E. Iborra, and J. Sangrador, "Wide bandwidth Bragg mirrors for multi-band filter chips," in *Proc. 2009 IEEE Int. Ultrasonics Symp.*, pp. 2119–2122.

[7] C.-J. Chung, Y.-C. Chen, C.-C. Cheng, and K.-S. Kao, "Fabrication and frequency response of solidly mounted resonators with $1/4\lambda$ mode configuration," *Thin Solid Films*, vol. 516, pp. 5277–5281, Jun. 2008.

[8] R. Aigner, J. Kaitila, J. Ella, L. Elbrecht, W. Nessler, M. Handtmann, T.-R. Herzog, and S. Marksteiner, "Bulk-acoustic-wave filters: Performance optimization and volume manufacturing," in *Proc. 2003 IEEE Int. MTT-S Digest*, pp. 2001–2004.

[9] S. H. Kim, J. H. Kim, J. K. Lee, S. H. Lee, and K. H. Yoon, "Bragg reflector thin film resonator using aluminium nitride deposited by RF sputtering," in *Proc. 2000 IEEE Microwave Conf. Asia-Pacific*, pp. 1535–1538.

[10] J.-W. Lobeek, R. Strijbos, A. Jansman, N. X. Li, A. B. Smolders, and N. Puisford, "High-Q BAW resonator on Pt/Ta$_2$O$_5$/SiO$_2$-based reflector stack," in *Proc. 2007 IEEE International MTT-S Digest*, pp. 2047–2050.

[11] H. P. Loebl, C. Metzmacher, R. F. Milsom, R. Mauczok, W. Brand, P. Lok, A. Tuinhout, and F. Vanhelmont, "Narrow band bulk acoustic wave filters," in *Proc. 2004 IEEE Int. Ultrasonics Symp.*, pp. 411–415.

[12] P. Emery, G. Caruyer, R. Vélard, N. Casanova, P. Ancey, and A. Devos, "Picosecond ultrasonics: An original tool for physical characterization of Bragg reflectors in bulk acoustic wave resonators," in *Proc. 2005 IEEE Int. Ultrasonics Symp.*, pp. 906–909.

[13] J. Olivares, E. Wegmann, J. Capilla, E. Iborra, M. Clement, L. Vergara, and R. Aigner, "Sputtered SiO$_2$ as low acoustic impedance material for Bragg mirror fabrication in BAW resonators," *IEEE Trans. Ultrason. Ferroelectr. Freq. Control*, vol. 57, no. 1, pp. 23–29, Jan. 2010.

[14] A. P. Huang, S. L. Xu, M. K. Zhu, B. Wang, and H. Yan, "Crystallization control of sputtered Ta$_2$O$_5$ thin films by substrate bias," *Appl. Phys. Lett.*, vol. 83, no. 16, pp. 3278–3280, Oct. 2003.

[15] C. Ferrari, A. Libassi, B. K. Tanner, V. Stolojan, J. Yuan, L. M. Brown, S. E. Rodil, B. Kleinsorge, and J. Robertson, "Density, sp^3 fraction, and cross-sectional structure of amorphous carbon films

determined by X-ray reflectivity and electron energy-loss spectroscopy," *Phys. Rev. B*, vol. 62, no. 16, pp. 11089–11103, Oct. 2000.

[16] J. F. Rosenbaum, *Bulk Acoustic Wave Theory and Devices*, Boston, MA: Artech House, 1988.

[17] P. Emery, A. Devos, and P. Ancey, "Picosecond ultrasonics: The preferred tool for BAW characterization," in *Proc. 2008 IEEE Int. Ultrasonics Symp.*, pp. 2205–2208.

[18] A. Devos, J.-F. Robillard, R. Côte, and P. Emery, "High laser-wavelength sensitivity of the picosecond ultrasonic response in transparent thin films," *Phys. Rev. B*, vol. 74, no. 6, art. no. 064114, Aug. 2006.